

# Micromirror for Laser-Beam Scanning for Robotics and Other Applications

David. J. Johnson

Institute of Information Sciences and Technology,  
Massey University, Palmerston North, New Zealand

[davidjohnson@sp.edu.sg](mailto:davidjohnson@sp.edu.sg)

Cassandra Low Lee Ngo

School of Electrical and Electronic Engineering,  
Singapore Polytechnic, Singapore

Jiaping Yang, Qinghua Li

Data Storage Institute, A\*STAR, Singapore

## Abstract

An electrostatically actuated torsional micromirror has been designed, fabricated and tested. The application of the micromirror device is for use as part of a Laser Beam Scanning (LBS) system. LBS systems can have a wide range of applications in many areas of science and technology, including a number of important applications relevant to the area of robotics and autonomous agents, such as automated control systems, robotic laser surgery, object identification, target tracking, display systems, etc. The proposed micromirror has been fabricated using wafer fabrication techniques, based on the bulk-micromachining method. Anodic wafer bonding between silicon and glass substrates have been also employed. Deep Reactive Ion Etching (DRIE) of a silicon substrate has formed the micromirror structure. The fabrication process is detailed in the paper. The test results of a fabricated prototype are presented and compared with the design parameters.

**Keywords:** beam positioning, beam scanning, MEMS, micromirror, electrostatic actuation, wafer fabrication

## 1 Introduction

Optical scanning has a wide range of applications in many areas of science and technology. These include a number of important applications relevant to the area of robotics and autonomous agents, such as automated control systems, robotic laser surgery, object identification, target tracking, display systems, etc. [1-4].

The intended application is to use a MEMS (Micro-Electromechanical System) actuator as part of a beam scanning system. Precise control of a laser beam is possible (Figure 1).

In comparison to conventional scanners, a MEMS micromirror based beam scanner has the potential to achieve high scan frequencies. Other benefits include low acoustic noise and low power consumption. By incorporating a MEMS micromirror, the existing scanner design can be miniaturized, widening the application area of the scanner [4].

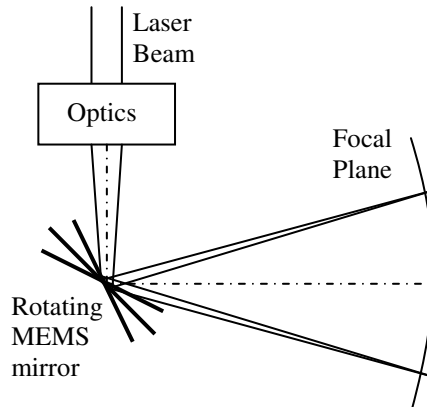


**Figure 1:** MEMS mirror as part of laser beam scanning system.

## 2 Scanning Mirror Design

A torsional micromirror has been designed employing electrostatic actuation. Electrostatic actuation is favoured over other actuation methods such as piezoelectric, thermal or magnetic [5]. Electrostatic torsional actuation of micromirrors has been examined in some detail in the past [6-8].

The micromirror designed is shown in Figure 2, all dimensions are in  $\mu\text{m}$ .

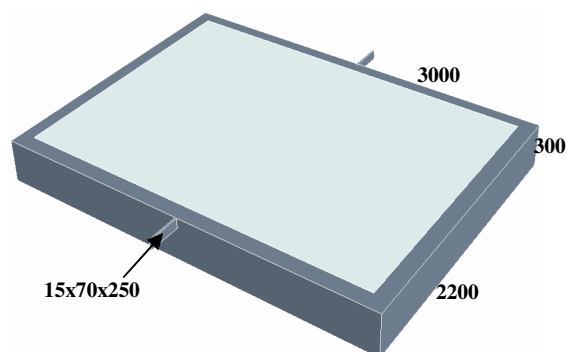


**Figure 2:** Torsional MEMS micromirror.

The micromirror has a large surface area (2.2mm x 3mm) that allows a range of lasers with different light volume diameters. The surface of the mirror is a thin aluminium film. Aluminium has good reflective properties over a range of light wavelengths [9].

Device performance of the MEMS micromirror is listed in Table 1.

**Table 1:** Micromirror device performance.

Max Rotational Angle:	0.27 degrees
Pull-in voltage:	13.7 at 0.12 degrees
1 <sup>st</sup> Resonant Freq:	600 Hz

### 3 Fabrication of Scanning Micromirror

#### 3.1 Device Requirements

To electrostatically actuate the mirror, a pair of aluminium electrodes are located below the mirror plate. The mirror will be at ground, a voltage is applied to an electrode. The mirror plate is attracted toward the electrode, rotating about the torsional beams.

The gap between the electrodes and the mirror is 7 $\mu$ m. Each electrode is approximately half the size of the mirror plate. In order to provide support to the actuating electrodes below the mirror plate, anodic bonding will be used to bond a Pyrex 7740 glass wafer to the underside of the silicon wafer containing the mirror structure [10].

Suitable space needs to be allowed for pad connection to the electrodes on the glass substrate, after anodic bonding. This space is provided to the left and right of the mirror plate.

#### 3.2 Process Development

Silicon wafers were chosen based on the need for the 300 $\mu$ m thickness requirement. Table 2 gives the characteristics of the wafers.

**Table 2:** Characteristics of the wafers for micromirror fabrication.

Type	Double side polished
Size	4 inch (100mm)
Thickness	300 $\pm$ 15 $\mu$ m
Doping	P/Boron
Crystal orientation	<100>
Resistivity	1-20 $\Omega$ -cm (test grade), 0.001-0.05 $\Omega$ -cm (final design)

Different methods of forming the gap were considered, including etching into the glass wafer, providing a thin structural layer (e.g. photoresist or similar polymer) or etching into the silicon substrate. This final method was decided upon as it was more feasible given available equipment.

The bulk micromachining technique of fabrication is to be used. This method involves the formation of the MEMS device by etching into the substrate by either wet or dry etching techniques [11]. Dry etching is done via a Surface Technology Systems Advanced Silicon Etch system. Typical etch rates with this machine are 2 to 3 $\mu$ m/min [12]. The mirror is to be etched out of the surrounding substrate, leaving only the beams supporting the mirror plate.

Three deep etches, of different depths, form the mirror structure. From the top side of the wafer a 70 $\mu$ m etch forms the beam. On the bottom side, an etch of 7 $\mu$ m forms the gap between the electrodes and the mirror. A 230 $\mu$ m deep etch on the bottom side meets the top side etch, allowing the mirror to move. The 7 $\mu$ m etch is over the same area as the 230 $\mu$ m etch, therefore the 230 $\mu$ m etch is reduced to 223 $\mu$ m.

Investigation into the process sequence order determined that it would be more viable to perform the bottom side etching first (223 $\mu$ m then 7 $\mu$ m) followed by the topside etch (70 $\mu$ m).

#### 3.3 Mask Design

The creation of three different masks is needed for the three etch steps. A fourth mask is needed for the patterning of the aluminium reflective layer on the mirror surface. A fifth mask is needed to pattern the aluminium electrode layer on the glass wafer. The CAD component of CoventorWare2003 MEMS design software is used to draw each mask. The masks were written using a DWL-66 mask writer.

Additional mirror designs were proposed. A groove pattern was designed to investigate air damping effects. Figure 3 shows the two different die designs for the second mask.

The die for the designed configurations are arranged on each mask. The number of die is kept quite low so that the wafer will remain relatively strong after processing. This also allows space for dicing later. Alignment features are also added to each mask.

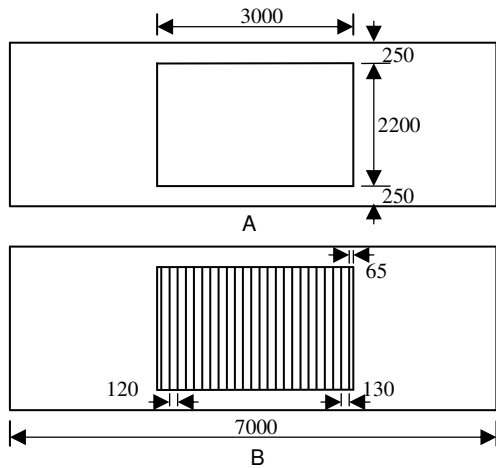


**Figure 3:** Second mask in fabrication process for 223µm etch, (A) original design, (B) with grooves for damping.

### 3.4 Process Flow

The final process flow is given in Figure 4.

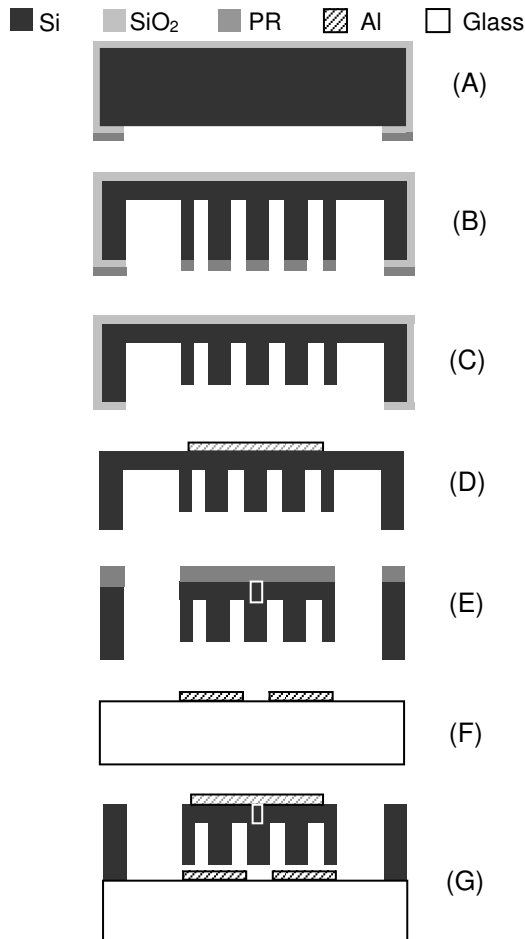


**Figure 4:** Final Process Flow.

Referring to Figure 4: in (A), a silicon dioxide layer is grown by thermal oxidation method in a diffusion furnace. The oxide is patterned using photolithography with the mask for the gap etch. The oxide is then etched using a reactive ion etch system. In (B), a protective photoresist layer is patterned by

the deep etch mask (223µm), then the silicon substrate is etched. In (C), the previous photoresist layer is removed, then the etch for the 7µm gap is run using the oxide mask. The oxide layer is then removed by HF acid. In (D), aluminium is deposited by DC sputtering. Photoresist is patterned using the reflective surface mask, and the exposed aluminium is etched. In (E), following patterning, the 70µm top etch is run. In (F), aluminium is sputtered onto the glass substrate and patterned using the electrode mask. (G) both wafers are bonded together using anodic bonding. Additional wafer cleaning processes are needed throughout the process for the removal of photoresists and other materials.

Clariant AZ 1512 photoresists are used for patterning the metal and silicon dioxide layers. Due to the duration of the 223µm and 70µm etch, Clariant AZP4620, a thick photoresist, is used as the masking material. Anodic wafer bonding (Figure 5) between the glass and silicon uses a voltage (300-700V), temperature (200-500°C) and vacuum to bond the two wafers firmly [11].

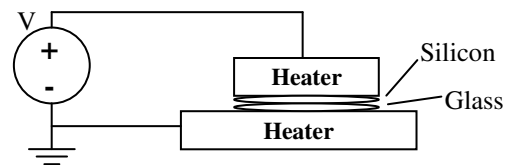


**Figure 5:** Anodic bonding system diagram.

## 4 Results

### 4.1 Fabrication Results

The fabrication was completed successfully for a number of sample silicon wafers. Figure 6 is a SEM photo showing the micromirror structure and surrounding substrate prior to anodic bonding. Figure 7 shows the damping grooves, the beam is visible on the right. Figure 8 is a close-up view of the beam. Some misalignment is visible with the groove below.

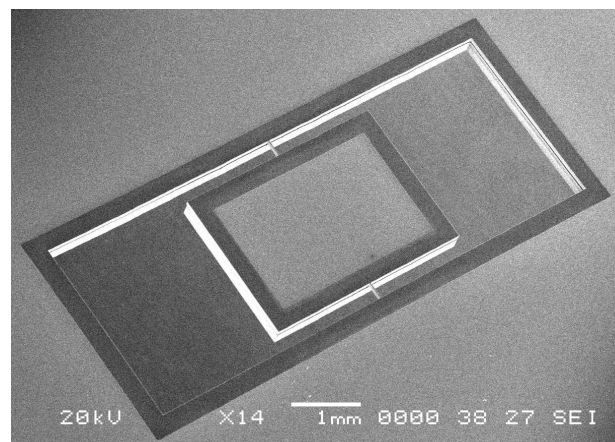


**Figure 6:** Micromirror structure on silicon wafer.



**Figure 7:** Mirror with damping grooves, the beam is visible to the right of the photo.

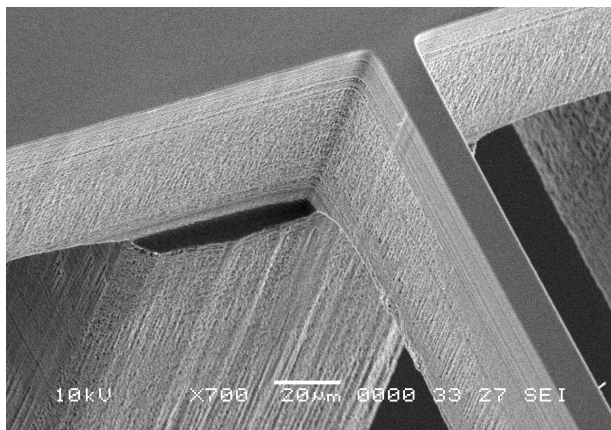


**Figure 8:** Close-up view of beam.

## 4.2 Prototype Testing

A prototype micromirror was successfully fabricated. Figure 9 shows a plan view of the mirror structure after bonding with glass substrate. Numerous anodic bonding attempts with the wafer samples resulted in breakage of the mirror structure.

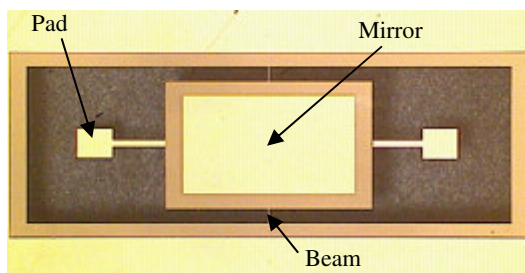


**Figure 9:** View of mirror device after bonding.

A probe station and an impedance analyzer are used to measure the capacitance vs. voltage (C-V) curve. The result is shown in Figure 10. By measuring the capacitance value  $C_0$  at driving voltage  $V = 0$ , it is estimated that the gap is  $7.05 \mu\text{m}$ , which is close to the designed value  $7.0 \mu\text{m}$ .

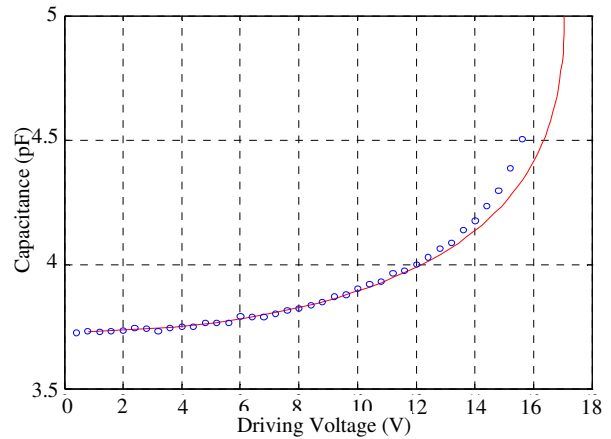


**Figure 10:** C-V curve measured for the MEMS mirror prototype.

A Laser Doppler Vibrometer (LDV) (Figure 11) is used to measure the static rotation angle of micromirror under the applied.

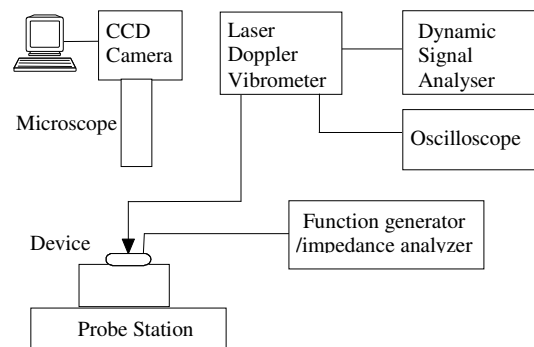


**Figure 11:** LDV Experimental Setup.

The mirror static rotation angle values vs. the varying voltages as shown in Figure 12.

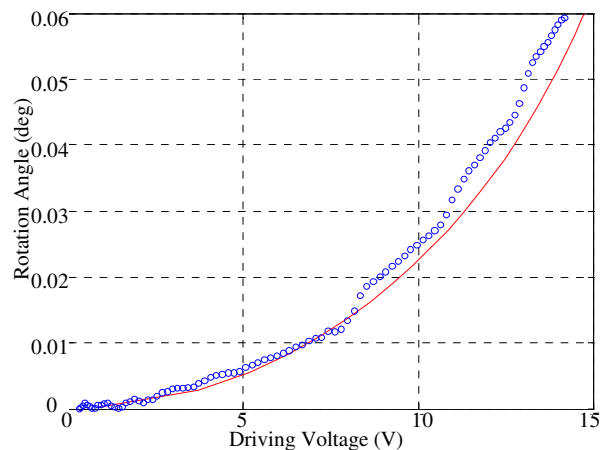


**Figure 12:** Measured curve of rotation angle vs. driving voltage.

Figure 13 shows the frequency response. The resonant frequency measured is 599 Hz and consistent with the designed 600 Hz.

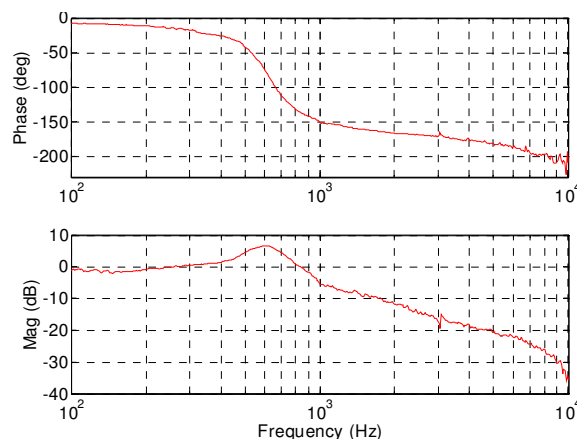


**Figure 13:** Frequency response measured for micromirror.

## 5 Discussion and Conclusions

An electrostatically actuated laser-beam scanning micromirror has been developed. A prototype based on a novel fabrication process was successfully fabricated and tested.

The fabrication process requires further development to improve repeatability. The anodic bonding of the wafers still remains a critical step. Many bonding attempts resulted in the breakage of the micromirror structure from the surrounding substrate.

Other fabrication process flows for the micromirror device is under investigation, to identify if there is a more robust fabrication method.

Differences in the test result in Figures 10 and 12 are the result of errors in the fabrication process. It is a challenge to control the gap distance to exactly  $7\mu\text{m}$ , further process optimisation of the DRIE etching will reduce these errors. The frequency response observed in Figure 13 is very close to that determined in the design of the device.

## 6 References

- [1] Kiang, M., etc., "Electrostatic combdrive-actuated micromirrors for laser-beam scanning and positioning", *Journal of Microelectromechanical Systems* Vol. 7(1), pp 27-37 (1998).
- [2] Yee, Y. J., etc., "Fabrication and characterization of a PZT actuated micromirror with two-axis rotational motion for free space optics", *Proceedings of the 14<sup>th</sup> IEEE Int. Micro Electro Mechanical Systems Conference*, pp 317-320, (2001).
- [3] Ueda, S., etc., "A micromachined tracking mirror for high-density optical disk memory", *Proceedings of Optical MEMS 2001*, pp 67-68 (2001).
- [4] Schenk, H., etc., "An electrostatically excited 2d-micro-scanning-mirror with an in-plane configuration of the driving electrodes", *Proceedings of the 13<sup>th</sup> IEEE Int. Micro Electro Mechanical Systems Conference*, pp 473-478, (2000).
- [5] Maluf, N., *An Introduction to Microelectromechanical Systems Engineering*, ARTECH HOUSE, Massachusetts, (2000).
- [6] Degani, O., etc., "Pull-In Study of an electrostatic torsion microactuator", *Journal of Microelectromechanical Systems*, Vol. 7 (4), pp 373-379, (1998).
- [7] Patterson, P.R., etc., "MOEMS electrostatic scanning micromirrors design and fabrication", *201st Meeting of the Electrochemical Society*, pp 369-380 (2002).
- [8] Camon, H., etc., "Analytical Simulation of a 1D Single Crystal Silicon Electrostatic Micromirror", *Proceedings of the International Conference on Modeling and Simulation of Microsystems*, pp 628-631, (1999).
- [9] Weber, M.J., *Handbook of optical materials*, CRC Press, Florida (2003).
- [10] Senturia, S.D., *Microsystem Design*, Kluwer Academic Publishers, Massachusetts, (2001).
- [11] Madou, M.J., *Fundamentals of Microfabrication*, 2nd Edition, CRC Press, Florida (2002).
- [12] Surface Technology Systems Corporate Website, <http://www.stsystems.com>, visited on 25/8/2004.